Res. Rep. Fac. Eng. Mie Univ., Vol. 21, pp. 55−67 (1996)

Review

Third-Order Optical Nonlinearity of Glass-Based Materials

Hiroyuki NASU and Kanichi KAMIYA
(Department of Chemistry for Materials)

(Received September 13 ,1996)

Abstract

Third-order optical nonlinearity of glass-based materials was measured by third-harmonic generation and degenerated four wave mixing method. In nonresonant-type nonlinear glasses, third-order nonlinearity is basically depending on the refractive index. On the other hand, in resonant-type glasses the magnitude of $\chi^{(3)}$ is as large as 10^{-8}esu, which is comparable the bulk semiconductor without slow decay time.

Key words: optical nonlinearity, glass-based materials, homogeneous glasses, refractive index, semicondouctor-doped glasses

1. Introduction

Semiconductor electronic devices are indispensable for the current electronics systems. Industries, markets, mass media and also our daily life are extensively based on the devices, and thus we are in, so called "electronics era". Nowadays, economics, politics industries and researches come to be borderless and information and various kinds of data will be expected to be enormous. To select and arrange the data for the users, ultra fast processing must be required. For electronic devices, the limit of the response time is intrinsically n sec or sub n sec order. To break the limit, all optical system should be developed since the responce time can be p or f sec order. Further, possible

parallel processing is also a significant advantage. These kinds of all optical system is called as photonic system, and the development of the new materials for photonics is strongly demanded.

The electric field ($E(\omega)$ dependent polarization ($P(\omega)$) is expressed as

$$P(\omega)=\chi^{(1)}(\omega)E(\omega))+\chi^{(2)}(\omega=\omega_1+\omega_2)E(\omega_1)E(\omega_2)+\chi^{(3)}(\omega=\omega_1+\omega_2+\omega_3)E(\omega_1)E(\omega_2)E(\omega_3)+\cdots \quad (1),$$

where, $\chi^{(1)}$ is the linear optical susceptibility and $\chi^{(2)}$ and $\chi^{(3)}$ and so on are the optical nonlinear susceptibilities. $\chi^{(1)}$ relates to the linear refractive index n_0 as

$$\chi^{(1)}=\frac{n_0^2-1}{4\pi} \quad (2)$$

Among the nonlinear susceptibilities, $\chi^{(2)}$ and $\chi^{(3)}$ are quite important from the magnitude and the functioning. $\chi^{(2)}$ causes second harmonic generation, parametric mixing and Pockels effect. $\chi^{(2)}$ intrinsically exists in the materials without inversion symmetricity. On the other hand, $\chi^{(3)}$ can be seen in every materials, and results in third harmonic generation, Raman and Brillouin scattering and various wave mixing processes including degenerate four wave mixing. In particular, optical Kerr effect is important since the intensity dependent refractive index results from the effect. The total refractive index (n) is expressed using the linear refractive index, nonlinear coefficient (n_2) and the time average square of the electric field ($\langle E^2 \rangle$) as

$$n=n_0+n_2\langle E^2\rangle \quad (3),$$

and n_2(esu) relates to real part of $\chi^{(3)}$(esu) ($\mathrm{Re}\chi^{(3)}$) as

$$n_2=\frac{12\pi}{n_0}\mathrm{Re}\chi^{(3)}_{1111}(-\omega:\omega,\omega,-\omega) \quad (4)$$

Using this effect, a number of all-optical devices such as shutter, self-modulator and rotator seem to be realizable. $\chi^{(3)}$ itself is expressed as a complex form,

$$\chi^{(3)}=\mathrm{Re}\chi^{(3)}+i\mathrm{Im}\chi^{(3)} \quad (5)$$

The origins of $\mathrm{Re}\chi^{(3)}$ are called non-resonant type and the others are resonant-type. Among those, the effects with the fast response time and relaxation time and the large $\chi^{(3)}$ are preferable. From this requests, nonlinear electron polarization for the non-resonant type and semiconductor band filling and exciton effect for the resonant type

effect can be picked up. Currently, several kinds of materials are candidates for $\chi^{(3)}$ materials, which are organics, semiconductors, liquids, gasses and ceramics including glasses. The general advantages of the glasses are high transparency, ease of fabrication to fibers or waveguides, thermal and chemical stability and high mechanical strength. Thus, glasses can be considered to have high potential for the practical use. This paper reports the development of high $\chi^{(3)}$ materials in non-resonant and resonant type.

2.Experiments

2.1 Non-resonant type homogeneous glasses

$\chi^{(3)}$ of the homogeneous glasses was evaluated by the third-harmonic generation (THG) method. Various homogeneous glasses were used for the THG measurement. Those were typical chalcogenides (As_2S_3, GeS_3 and 90(mol%)GeS_2·10(mol%)Tl_2S), chalcohalides (98(mol%)As_2S_3·2(mol%)I), tellurites ($PbO-TiO_2-TeO_2$, $Li_2O-TiO_2-TeO_2$), germanates (Na_2O-GeO_2), silicates(Na_2O-SiO_2, Li_2O-SiO_2, K_2O-SiO_2, Rb_2O-SiO_2, Cs_2O-SiO_2) and CdO-containing glasses, which were prepared from commercially available, analytical-grade As, S, Ge Tl_2S, I, PbO, TiO_2, TeO_2, Li_2CO_3, Na_2CO_3, K_2CO_3, Rb_2CO_3, Cs_2CO_3, CdO, GeO_2 and SiO_2 powders. After weighing, the chalcogenide and chalcohalide glasses were prepared in evacuated and sealed silica ampoules in an electric furnace from 850-900°C and quenched in air to room temperature. For oxide glasses, after weighing the raw materials were mixed and put into Pt-Au crucibles for tellurites and Pt crucible for the others, and then melted in air from 850-900°C for tellurites and from 1450-1550°C for the others for about 1h. The melts were subsequently quenched in air to room temperature. The surfaces of the bulk glasses obtained were polished to eliminate surface light scattering.

The THG values of the glasses were measured using a pump wavelength of 1.9μm generated from an H_2 raman shifter excited by a Q-switched Nd:YAG laser. The pump duration was 5.5ns, the repetition rate was 10Hz, and the peak power density was 200MW/cm^2. The details of the experiment can be found elsewhere [1].

2.2 Resonant type semiconductor microcrystal-doped glasses

Semiconductor microcrystals dispersed in a transparent matrix can exihibit a high resonant-type third-order nonlinearity. Even as a matrix, glasses are superior to other materials such as organic polymers because of thermal and chemical stability and excellent hardness and rigidity. Microcrystals of several semiconductor such as CdTe, CdSe, PbS, GaAs, Ge and Si dispersed in SiO_2 glass thin films were prepared by a conventional magnetron rf-sputtering method. Suitable sputtering conditions depend on the semiconductor dopants, except for

the sputter gas (pure Ar), the pressure (~10^{-2}Torr), the target and substrate separation (50mm), sputtering time, and the SiO_2 target of 10cm in diameter located beneath the semiconductor chips. For instance, the mean diameter and size distribution of CdSe microcrystals depend on the input rf power, the substrate temperature and the relative surface area of CdSe chips to that of SiO_2 target. The influences of those parameters are shown in the Result section. The substrates used were SiO_2 glasses, KBr or single crystals of so-called offset Si which show no intense X-ray diffraction peak.

The mean size and size distribution of microcrystals were determined by two methods. One was the estimation from the full width at half maximum (FWHM) of the X-ray diffraction (XRD) lines and the second was the direct observation using transmission electron microscopy (TEM). For the first method, films on off-set Si crystals were used. The XRD patterns were recorded by Shimadzu XD-610 diffractometer with Ni filtered Cu Kα radiation as a source. The patterns were obtained by step scanning with 0.05° steps and 40s accumulation time. No significant fluctuation was found for the mean size evaluated from several times scanning. TEM measurements were performed with a Hitachi H-800 microscope. The semiconductor-doped films on KBr pellets were soaked in distilled water to dissolve the KBr substrates, and then the insolubles were put on a copper mesh. No crystal growth during TEM observation was seen in this experiment. The size distribution was determined from tens of pictures taken at the various points, and measurement error was ± 0.5Å. The optical absorption spectra were measured for the films on SiO_2 glass substrates with a Shimadzu UV-3100 spectrometer at room temperature in air. The reproducibility of the spectra were confirmed by several scannings. Film thicknesses were obtained from scanning electron microscope (SEM; Hitachi S-2300) pictures. X-ray photoelectron spectroscopy (XPS; Shimadzu ESCA 750) was used to examine chemical bonding states and composition of the films.

For the resonant-type glasses, THG is not available, and thus $\chi^{(3)}$ and delay time were measured by the degenerate four wave mixing (DFWM) technique at the 532nm second harmonic generation of a Nd:YAG laser. The detail can be found elsewhere [2].

3.Results

3.1 Non-resonant type homogeneous glasses

As pointed out in the Introduction, more or less every homogeneous glasses have $Re\chi^{(3)}$. To develope glasses with large $Re\chi^{(3)}$ several semiemprical rules are very useful. For instance, Miller's rule, which is quite convenient in designing a glass composition with high $Re\chi^{(3)}$, is

$$Re\chi^{(3)}=(\chi^{(1)})^4 \times 10^{-10} \text{ (esu)} \qquad (6).$$

Table 1
$\chi^{(3)}$ and refractive index of some high-index glasses

Glass composition	$\chi^{(3)}$(esu)	Refractive index (633nm)
Chalcogenide glasses		
As_2S_3	7.2×10^{-12}	2.53
NOG-1(Ge-S)	2.0×10^{-12}	2.05
NOG-2(Ge-As-S)	3.7×10^{-12}	2.22
NOG-3(Ge-As-S)	4.6×10^{-12}	2.35
NOG-4(Ge-As-S-Se)	7.0×10^{-12}	2.36
NOG-5(As-S-Se)	1.4×10^{-11}	2.55
Tellurite glasses		
$20Li_2O\cdot5TiO_2\cdot75TeO_2$	4.3×10^{-13}	2.1
$10Li_2O\cdot10TiO_2\cdot80TeO_2$	8.0×10^{-13}	2.2
$10PbO\cdot10TiO_2\cdot70TeO_2$	2.8×10^{-12}	2.20
$25PbO\cdot10TiO_2\cdot65TeO_2$	3.7×10^{-12}	2.27
$20PbO\cdot5TiO_2\cdot75TeO_2$	3.6×10^{-12}	2.13
$10Nb_2O_5\cdot10TiO_2\cdot80TeO_2$	1.2×10^{-12}	2.18
$15Nb_2O_5\cdot10TiO_2\cdot75TeO_2$	9.6×10^{-13}	2.27
TeO_2	1.4×10^{-12}	2.239
Gallate glasses		
$67PbO\cdot33GaO_{1.5}$	7.7×10^{-13}	2.260
$10TiO_2\cdot60PbO\cdot30GaO_{1.5}$	8.5×10^{-13}	2.301
RN	4.2×10^{-13}	2.30
Germanate glasses		
GeO_2	1.0×10^{-13}	1.645
$20Na_2O\cdot80GeO_2$	1.3×10^{-13}	1.678
Silicate glasses		
SiO_2	2.8×10^{-14}	1.45
lead silicate glasses	$4.4\text{-}7.5\times10^{-14}$	1.7-2.02
$NbO_{5/2}$-TiO_2-Na_2O-SiO_2	$0.7\text{-}5.8\times10^{-14}$	1.54-1.95

Thus, glasses with high refractive index are expected to have high $Re\chi^{(3)}$. The $\chi^{(3)}$ values obtained for various high index glasses are tabulated in Table 1. In paticular, chalcogenide glasses have relatively large values, and the largest can be seen for As_2S_3 (7.2×10^{-12} esu) and As-S-Se (1.4×10^{-11} esu) glasses, which is over 200 times

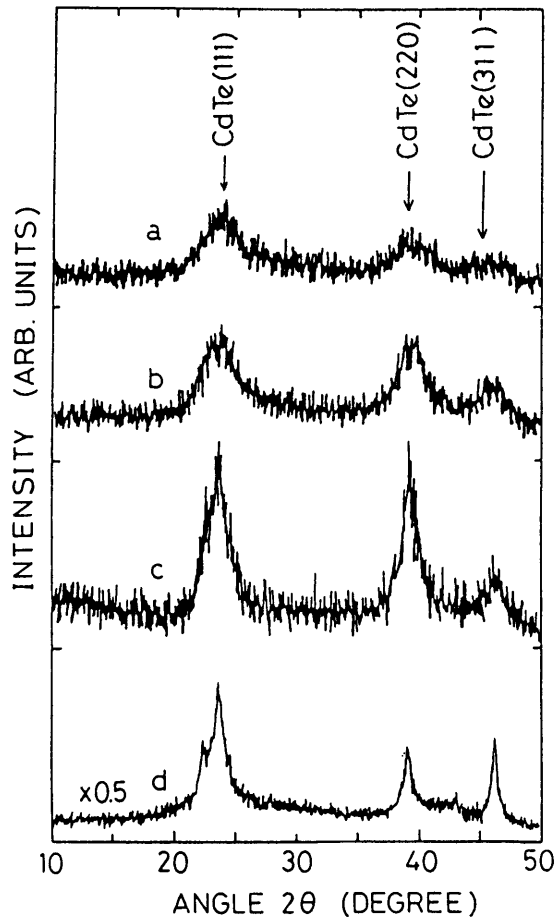

Fig. 1. XRD patterns of CdTe-doped SiO_2 glass thin films prepared by rf-sputtering method with the CdTe surface area of (a) 3.1%, (b) 4.2% and (c) 6.3%, located on the center of the target, and (d) 2.0% located 3 cm away from the center of the target.

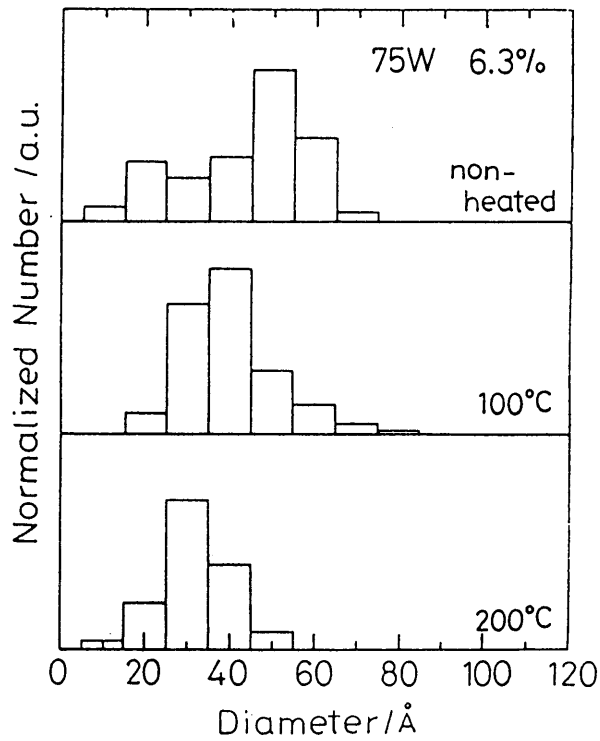

Fig. 3. Dependence of CdSe microcrystals size distribution on the substrate temperature.

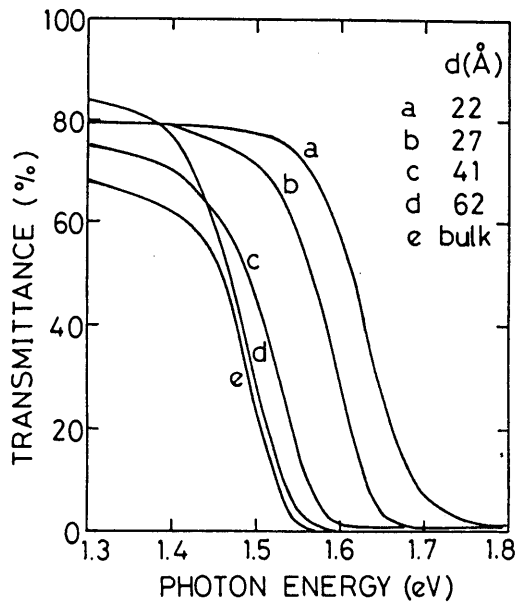

Fig. 2. Visible transmission spectra of the films shown in Fig. 1 with the same notation, and with a bulk CdTe crystal (e) for comparison.

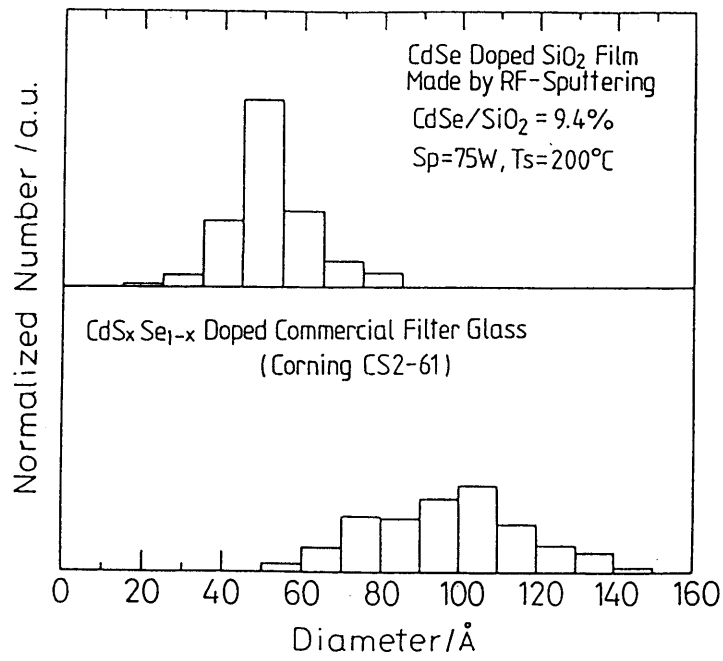

Fig. 4. Microcrystals size distribution of (bottom) commercial filter glass and (top) sputtered films after optimization.

larger than that of SiO_2 glass. Among oxide glasses, $\chi^{(3)}$ of tellurite glasses, especially $PbO-TiO_2-TeO_2$ glasses, is larger than that of the other oxide glasses.

3.2 Resonant type semiconductor microcrystal-doped glasses

Fig.1 shows the XRD patterns of as-deposited thin films prepared from the target with relative CdTe surface area of (a)3.1%, (b)4.2%, (c)6.3%, located directly on the center of the target, and (d) from the target with the relative surface area of 2.0% located 3cm away from the center of the target. One can see three peaks which are ascribed to the CdTe (111), (220) and (311) diffraction lines. All peaks in (a) are the broadest among the four films, and the mean diameter of the microcrystals was estimated to be 22 Å. As seen in this figure, the sharpness of each peak was significantly influenced by the relative surface area or the location of the chips. The mean diameter of the microcrystals were estimated to be 27Å for (b), 41 Å for (c) and 62Å for (d).

Fig. 2 depicts the visible transmission spectra of the films in Fig. 1 with a bulk CdTe crystal (e) for comparison. Compared with the of the crystal (e), the curve (a) containing microcrystals with the mean diameter of 22Å exhibited a blue shift of about 0.15eV. Similarly, blue shifts were observed for the other films and the shift incresed as microcrystal size decreased. This tendency establishes the quantum size effeft on the electronic energy levels of dopants, and thus the CdTe microcrystals in the films can be considered as quantum-dots. From XPS observation, no detectable oxidation during the sputtering process of any semiconductor can be seen.

Sputtering conditions influence the microcrystal size distribution as well as the mean size. The influence of the substrate temperature on the distribution for CdSe-doped glass film is shown in Fig. 3. As one can notice, the distribution becomes narrower as the temperature increases, although this tendency depends on the dopants. Fig. 4 compared an optimized distribution in the films with that of a commercial bulk filter glass. The size is mostly distributed in the range of 40-80Å for the films, and in the range of 50-150Å for the bulk filter glass. The difference is made more obvious in Fig.5. After the optimization, the standard deviation is almost independent of the mean diameter of the microcrystals, and is nearly half of that of the commercial filter glass.

The average DFWM signal as a function of the probe deley time, τ_d, for CdSe-doped films from the several times measurement is shwn in Fig.6. A coherent spike can be seen at delay time $\tau_d=0$ since the polarizations of the three beams are parallel. The DFWM signal as a function of τ_d shows biexponential behavior with a fast decay component and a slow decay component. The fasr and slow decay time (τ_f and τ_s)

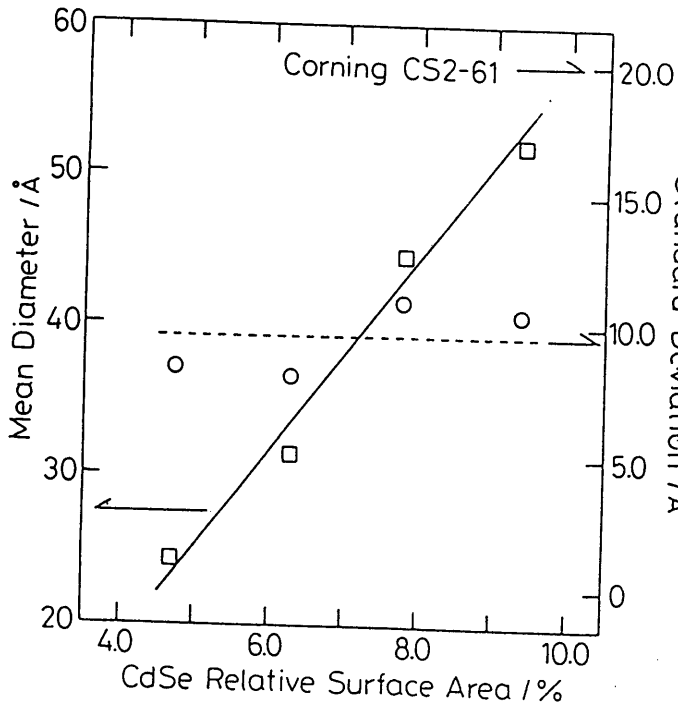

Fig. 5. The mean diameter and the standard deviation of size distribution for the sputtered films after optimization. The lines are the least squares fits.

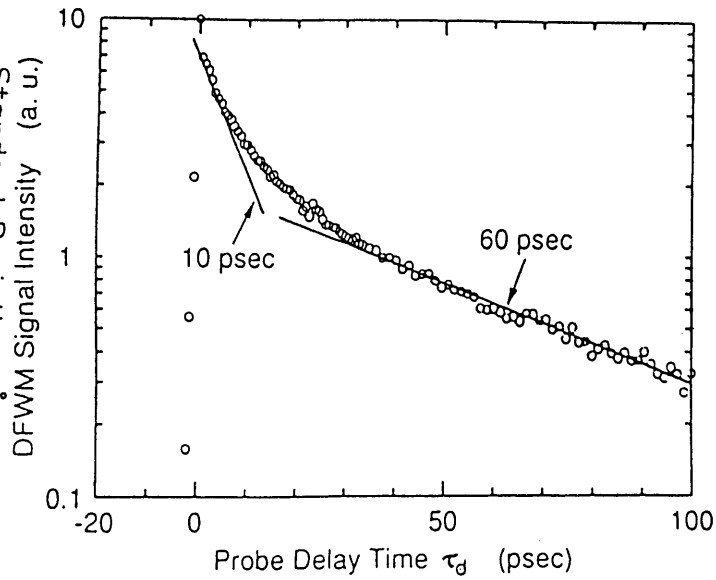

Fig. 6. DFWM signal as a function of the probe delay time [3].

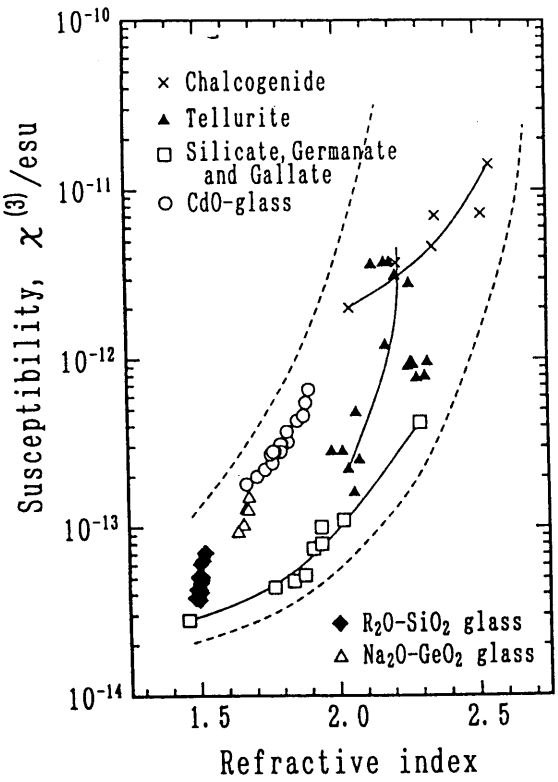

Fig. 7. $\chi^{(3)}$ of various glasses as a function of the refractive index. Lines are drawn as guides to the eye.

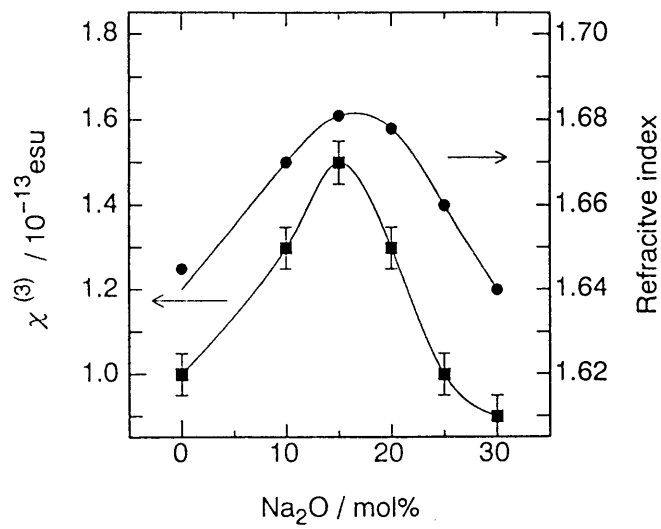

Fig. 8. $\chi^{(3)}$ and the refractive index as a function of the Na_2O content in the Na_2O–GeO_2 glass system. Lines are drawn as guides to the eye.

are 10 and 60±5 ps, respectively, and strength of the fast decay component is 1.4 times larger than that of the slow one. From these data, $|\chi^{(3)}|$ can be calculated to be 1.3×10^{-8}esu.

4.Discussion

4.1 Non-resonant type homogeneous glasses

Fig.7 shows $\chi^{(3)}$ of various glasses as a function of the refractive index. One can say that $\chi^{(3)}$ depends on the rafractive index as expected by Eq. (6), although a sigle n does't uniquely determine $\chi^{(3)}$.

To design glass composition with large $\chi^{(3)}$, an understanding of the contribution of each ion or ion group to $\chi^{(3)}$ is indespensable. Assuming that $\chi^{(3)}$ is caused by hyperpolarizability of the constituents, the dipole moment of an individual ion can be expressed as [3]

$$p(t)=\alpha^{(1)}E_{loc}(t)+(\alpha^{(3)}/6)(E_{loc}(t))^3 \qquad (7),$$

where p is the induced dipole moment of the ion, $\alpha^{(1)}$ is the polarizability of the ion, $\alpha^{(3)}$ is its hyperpolarizability, E_{loc} is the local delectric field on the ions and t is the time. For glasses, $\chi^{(3)}$ is re lated to $\alpha^{(3)}$ by [3]

$$\chi(-\omega;\omega_1,\ \omega_2,\omega_3)=\frac{L(\omega)L(\omega_1)L(\omega_2)L(\omega_3)}{24}\sum_i N_i\alpha^{(3)}{}_i \qquad (8),$$

where the subscript, i, stands for the contribution from constituenti, N_i is the number of i ions and $L(\omega)$ is related to the local electric field and frequently taken to be the Lorentz correction factor:

$$L(\omega)=(n_0{}^2+2)/3 \qquad (9),$$

which is exactly correct for a perfect ionic cubic crystalline solid [3].

Fig. 8 shows the composition dependence of $\chi^{(3)}$ for Na_2O–GeO_2 glasses which show the well-known "germanate anormaly". Just like the refractive index, $\chi^{(3)}$ shows a maximum at 15mol% Na_2O. In the Na_2O–GeO_2 glasses, GeO_4, GeO_6 and GeO_{3+NBO} (NBO stands for non-bridging oxygen) are known to exist. The contribute of each group to $\chi^{(3)}$ can be calculated using Eqs.(8) and (9), and $\alpha^{(3)}$ is 2.03×10^{-35} esu cm^3 for the GeO_4 unit , 4.87×10^{-35} esu cm^3 for the GeO_6 unit and 1.96×10^{-35} esu cm^3 for the GeO_{3+NBO} unit.

In alkali silicate glasses, NBO depends on the content of alkali ions. It is mathematically impossible to differenciate the $\alpha^{(3)}$ values of NBO and that of alkali ions since the ratio of NBO to alkali ions is unchangeable. Thus, it is neceassary to vary the ratio by adding other components to evaluate the contribution of each ion separatively. In

alkali aluminosilicate glasses, an Al ion consumes one NBO to form an AlO_4 tetrahedron, working as network former, when $Al_2O_3<1$ [4]. In additon, the values of $\chi^{(3)}$ and $\alpha^{(3)}$ of Al_2O_3 are quite close to those of SiO_2 [5], and thus the contribution of Al to $\chi^{(3)}$ can be quite similar to that of Si. In specific, $\chi^{(3)}$ of α-Al_2O_3 and SiO_2 glass are 2.9×10^{-14} and 2.8×10^{-14} esu, respectively. Thus, the influence of Al_2O_3 addition on $\chi^{(3)}$ can be negligible. Using th data for alkali silicate and alkali aluminosilicate glasses, the $\alpha^{(3)}$ of each chemical constituent was calculated to be (in esu cm^3)

$$a^{(3)}_{Si-O-Si(Al)}=0.43\times10^{-35},$$

$$\alpha^{(3)}_{Si-O}-=0.60\times10^{-35},$$

$$\alpha^{(3)}_{Na}+=0.6\times10^{-35},$$

$$\alpha^{(3)}_{K}+=1.0\times10^{-35},$$

$$\alpha^{(3)}_{Rb}+=2.2\times10^{-35}.$$

From the results, it can be noted that $\alpha^{(3)}$ of NBO is about 1.4 times larger than that of bridging oxygen. Further, the enlargement of the ion radius of alkali ion positively contributes to the enlargement of $\alpha^{(3)}$ and $\chi^{(3)}$. The values of $\alpha^{(3)}$ of Na^+ is comparable with that of NBO and those of K^+ and Rb^+ are even larger. Considering the bond nature in the glasses, the ionicity is the lowest in the bridging oxygens and the highest in alkali ions. The valence electron distribution can be considered to be mostly spherical in highly ionic ions, while they are mainly directional in highly covalent bonding. Therefore, the electrons of alkali ions may easily be distorted by the strong electromagnetic field compared with NBO and bridging oxygens. Further, the higher ionicity of non-bridging oxygen oxygens may result in higher $\alpha^{(3)}$ than the bridging ones. Among alkali ions, the larger ions are more polarizable and could have larger $\alpha^{(3)}$.

Fom above calculation, to design the large $\chi^{(3)}$ oxide glasses, the formation of the higher coordination state and the introduction of the highly ionic ions are found to be effective.

4.2 Resonant type semiconductor microcrystal-doped glasses

The change of the energy gap depending on the microcrystal radius by the quantum size effect can be divided into two categories [6]. When the radius, R, is much larger than the Bohr radius (r_B), $R/r_B>4$, exciton confinement occurs. In this case, the band gap shift (ΔE) can be written as

$$\Delta E=(\hbar/2M)(\pi/R)^2 \qquad (10),$$

and M is the translational mass as

$$M=m_e+m_h \quad (11),$$

where $\hbar=h/2\pi$; m_e and m_h are the effective mass of an electron and a hole, respectively. When $R/r_B<2$, elecron-hole confinement takes place and ΔE can be expressed as

$$\Delta E=(\hbar^2/2\mu)(\pi/R)^2 \quad (12),$$

and μ is th reduced mass as

$$1/\mu=(1/m_e)+(1/m_h) \quad (13).$$

In the case of CuCl-doped glasses (r_B=6.8Å), ΔE should follow Eq. (10) because of the small exciton radius, and actually the behavior satisfies Eq.(10) [7]. However, the present dopants have a much larger exciton Bohr radii. For instance, the Bohr radius of CdSe is 50Å, and thus it should follow he electron-hole confinement theory. Fig.9 shows the plots of ΔE versus the reciprocal square of the mean microcrystal radius, $1/R^2$, for CdSe-doped SiO_2 glass thin films with the theoretical curves of Eqs.(10) and (12). The experimental values including data in the literature [8] clearly deviate from both curves. Thus we use the equation proposed by Kayanuma [9],

$$\Delta E=\frac{h^2}{2\mu}\left(\frac{\pi}{R}\right)^2-1.786\frac{e^2}{\varepsilon R}-0.248R_y^* \quad (14),$$

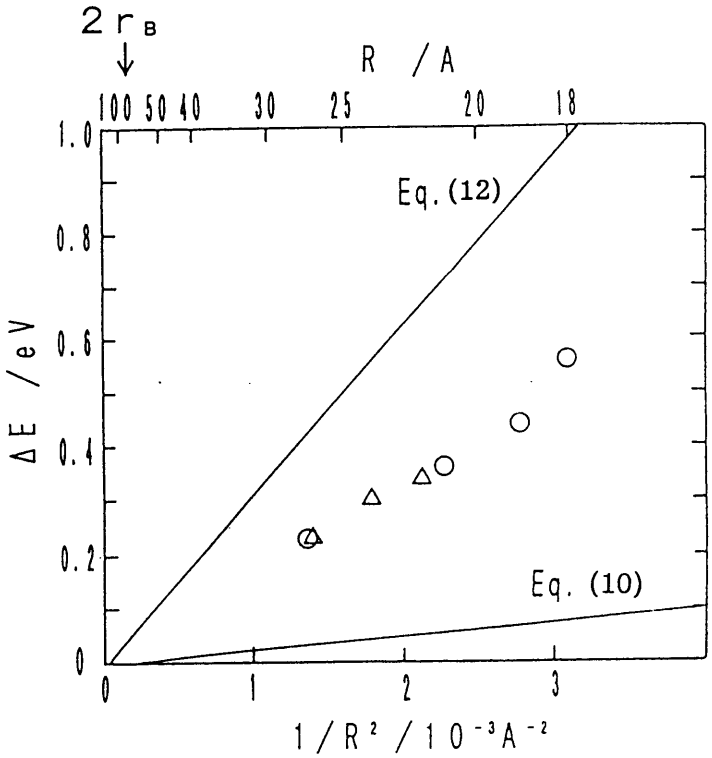

Fig. 9. Plots of the band gap shift, ΔE_g, as a function of the reciprocal square of the mean microcrystal diameter, $1/R^2$, with the theoretical curves. ○, present data; △, data in literature

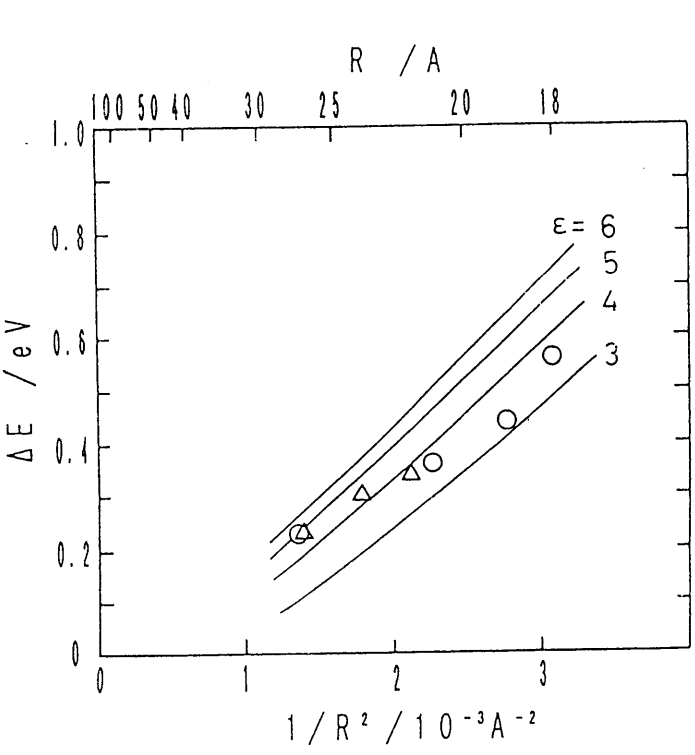

Fig. 10. Plots of ΔE_g as a function of $1/R^2$ with Kayanuma's theoretical curve using various values of ϵ from 3 to 6.

where ε is dielectric constant and R_y^* is effective Rydberg energy. When r_B is large enough compared with the polaron radius, $\varepsilon=\varepsilon_0$ (ε_0 is the static dielectric constant). Otherwise, $\varepsilon=\varepsilon_\infty$ (ε_∞ is the optical dielectric constant). The electron and hole polaron radii are estimated to be 33.8Å and 10.3Å, respectively, based on the angular frequency of the longitudinal optical phonon. Thus, ε should be ε_∞ since r_B for CdSe is 50Å. The plots of the curves obtained by varying ε from 3 to 6 based on ε_∞ of 2.1 for SiO_2 and 6.23 for CdSe, respectively, can be compared with the experimental data in Fig.10.

From this figure, it can be said that ε values between 3 and 5 yield good agreement with the experimental data, but the ε appears to depend on crystal radius, R. Therefore, the Haken potential relating the dependence of ε on particle size is used [10]

$$\frac{1}{\varepsilon(r^*)} = \frac{1}{\varepsilon} - \left(\frac{1}{\varepsilon} - \frac{1}{\varepsilon_0}\right)\times\left(1 - \frac{\exp(-r^*/\rho_1)+\exp(-r^*/\rho_2)}{2}\right) \qquad (15),$$

where ρ_1 and ρ_2 are the polaron radii of an electron and a hole, repectively. and r^* is the mean distance between electron and hole. $r^*=0.69932R$ was used in the present calculation. Fig.11 shows the curves for ε_∞ =6.23 (CdSe) and 2.1 (SiO_2). As one can notice, the good agreement of theory with the experiment can be seen when ε_∞ =2.1. It implies a significant role of the matrix on the quantum size effect for semiconductor microcrystals with large exciton radii (larger than the microcrystals).

5.Conclusion

The third-order nonlinearity of glasses of non-resonant type and resonant type was measured. From the results, following points are clarified. With respect to non-resonant type homogeneous glasses.

1) $\chi^{(3)}$ basically depends on the refractive index of the glasses.
2) The coordination state and ionicity influence $\alpha^{(3)}$.
3) The largest $\chi^{(3)}$ are in the order of 10^{-11} esu.

With respect to resonant type semiconductor microcrystal-doped glasses

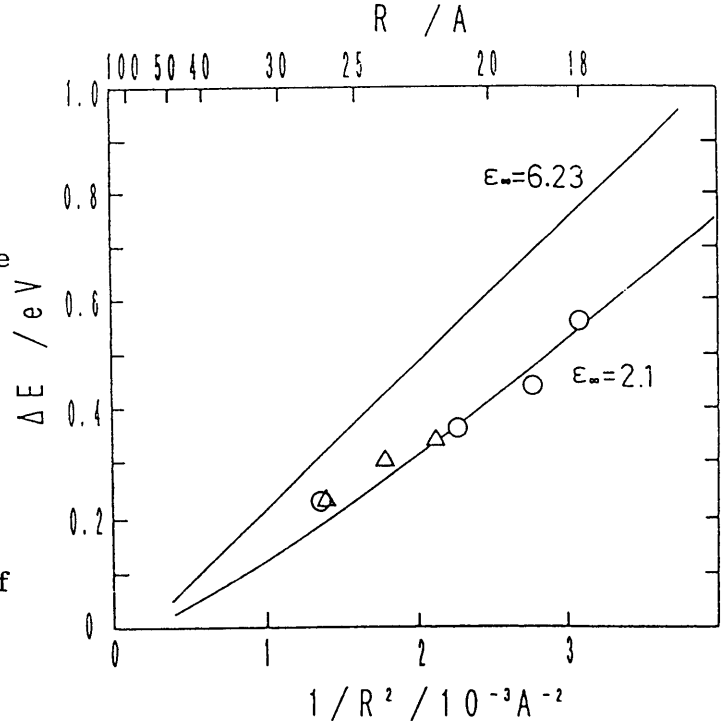

Fig. 11. Plots of ΔE_g as a function of $1/R^2$ with Kayanuma's theoretical curve using the Haken potential.

1) Quantum size effect is seen in band gap of doped semiconductor micro-crystals.
2) The size distribution is controlable by prepatation conditons.
3) The significant influence of the matrix on the quantum size effect is seen.

References

[1] H. Nasu, J. Matsuoka and K. Kamiya, J. Non-Cryst. Solids 178 (1994) 23.
[2] H. Nasu, J. Matsuoka and K. Kamiya, J. Non-Cryst. Solids 178 (1994) 148.
[3] N.F. Borrelli and D.W. Hall, in: Optical Properties of Glass, ed. D.R. Uhlmann and N.J. Kreidl (American Ceramic Society, Columbus, OH, 1991) p.87
[4] W.D. Kingery, H.K. Bowen and D.R. Uhlmann, Introduction to Ceramics (Wiley, New York, 1976) p.105.
[5] T. Hashimoto, T. Yoko and S. Sakka, J. Ceram. Soc. Jpn. 101 (1993) 64.
[6] Y. Maeda, N. Tsukamoto, Y. Yazawa, Y. Kanemitsu and Y. Masumoto Appl. Phys. Lett. 59 (1991) 3168.
[7] T. Manabe, N. Sugimoto and A. Nakamura, in Advanced Nonlinear Optical Organic Materials I, ed. H. Nakanishi, T. Kobayashi A. Nakamura and S. Umegaki (CMC, Tokyo, 1991) p.223.
[8] K. Tsuñetomo, H. Nasu, H. Kitayama, A. Kawabuchi, Y. Osaka and K. Takiyama, Jpn. J. Appl. Phys. 28 (1989) 1928.
[9] Y. Kayanuma, Phys. Rev. B38 (1988) 9797.
[10] H. Haken, Nuovo cim. 10 (1956) 1230.